ACS OMEGA

http://pubs.acs.org/journal/acsodf

Article

Molecular Characteristics of Jimusaer Shale Oil from Xinjiang, China

Luhao Chen, Jingmei Liu, Zhilei Wu, Jinsheng Liu, Aisha Nulahong,* and Fengyun Ma*

Cite This: *ACS Omega* 2022, 7, 35496−35505

Read Online

ACCESS | Metrics & More | Article Recommendations

ABSTRACT: Increasing attention is currently obtained by the exploitation and utilization of unconventional energy sources globally. Jimusaer shale oil (JSO) was prepared by dry distillation from oil shale in Jimusaer, Xinjiang, China. Using *n*-heptane and toluene as solvents, saturate (SA), aromatic (AR), resin (RE), and asphaltene (AS) samples were produced from JSO. Samples were subsequently analyzed by elemental analysis (EA), thermogravimetric analysis (TG-DTG), infrared analysis (FT-IR), high-performance gel chromatography (GPC), and nuclear magnetic resonance (^{1}H-NMR and ^{13}C-NMR). In terms of basic properties, element content, classification of combustible minerals, and refining performance, JSO, which has a high H/C value, low carbon residue yield, low metal content, and excellent refining-processing performance, is considered a high-quality shale oil compared with the shale oil produced in other areas. The refining performance of JSO is even comparable with petroleum. According to column chromatography, the contents of SA, AR, RE, and AS in JSO are 54.32, 18.86, 25.81, and 1.01%, respectively. The results of FT-IR and NMR (^{1}H-NMR and ^{13}C-NMR) demonstrated that the chain alkane or aromatic cycloalkyl substituents of SA, AR, and RE decrease sequentially, while the number of aromatic rings and cycloalkane rings and the degree of condensation increase sequentially. These results indicate that the chain alkanes with a small number of cycloalkanes are the main component of SA. The AR and RE contain more thick-ring aromatic hydrocarbons. According to GPC, the molecular weight (M_n) of JSO is 845 g·mol^{-1}, and those of SA, AR, and RE are 702, 1107, and 2218 g·mol^{-1}, respectively. The estimated molecular formulas (M_{af}) of JSO, SA, AR, and RE, which were calculated based on the combined results of GPC and EA, are $C_{57.91}H_{115.60}O_{1.38}N_{0.79}S_{0.04}$, $C_{48.02}H_{101.79}O_{0.69}N_{0.85}S_{0.03}$, $C_{76.96}H_{137.16}O_{1.08}N_{1.87}S_{0.09}$, and $C_{156.24}H_{247.75}O_{1.46}N_{4.42}S_{0.32}$.

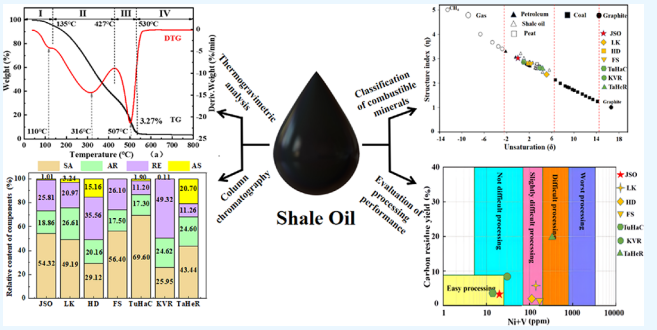

1. INTRODUCTION

Shale oil is a liquid fuel coming from the thermal decomposition of organic matter of oil shale. Although the hydrocarbon ratio of shale oil is similar to crude oil, it contains more unsaturated hydrocarbons and organic compounds including nitrogen, sulfur, and oxygen.[1,2] Shale oil in China is mainly distributed in the Ordos Basin, Songliao Basin, Bohai Bay Basin, and Junggar Basin.[3] The recoverable reserves of shale oil in Jimusaer of the Juggar Basin are estimated as 4.4 × 10^9 tons.[4] Given the global oil shortage and the exploitation, research, and utilization of shale oil, an unconventional energy substitution of oil is urgently needed.

Unconventional energy sources are attracting extensive attention in the past two decades. Therefore, research on the chemical composition and molecular structure of shale oil has been widely reported. Jarvis *et al.*[5] compared the compositional characteristics of shale oil, petroleum, and biomass oil by FT-IR-MS and found that the total hydrocarbon content of shale oil was close to that of petroleum but much higher than that of biomass oil. According to the FT-IR and NMR (^{1}H-NMR and ^{13}C-NMR) analysis, the saturated hydrocarbon of soluble matter of Jordanian shale oil dissolved by tetrahydrofuran and methylene chloride was about 85 and 11%.[6] Li[7] analyzed shale oil samples from Fushun and Nongan by GC−MS and found that the chemical compositions of both samples, which contained about 70% of linear and branched saturated alkane and 30% of arenes and oxygenate, were similar to each other. Cui *et al.*[8] analyzed shale oil samples collected from Huadian by GC−MS as well. According to their report, hydrocarbons accounted for 93% of the total composition, 60% of which was paraffin and the rest were olefins and monoaromatic hydrocarbons. Additionally, the sample also contained less than 5% of heteroatomic compounds such as sulfur, nitrogen, and oxygen. Mukhamatdinov *et al.*[9] studied the impact of aromatic solvents for enhancing heavy oil recovery from the Ashalcha field and found that when toluene:benzene = 1:1, the macromolecular structure inside the resin could be effectively

Received: February 28, 2022
Accepted: July 22, 2022
Published: September 27, 2022

Table 1. Basic Properties of JSO and Its Comparison with Other Samples

type	sample	ρ (kg/m^3) at 20 °C	A_d (%)	M (%)	FP (°C)	salt content (mg/L)	RC (%)	Ni (μg/g)	V (μg/g)	Fe (μg/g)	Ca (μg/g)
shale oil	JSO	899.3	0.32	0.15	15.0	2.74	3.27	21.25	0.32	0.69	15.54
	LK[12]	850.1	0.01	3.59	3.6		6.94	38.5	118.0		
	HD[13]	892.2	0.06	0.37	12.0		1.92	55.4	64.9		
	FS[14]	903.3	0.88	3.00	33.0		1.63	72.1	118.0		
petroleum	TuHaC	857.3				26.56	3.45	15.29	0.0	12.00	2.94
	KVR	944.2	0.09		2.0		8.15	31.80	0.75	56.60	588.2
	TaHeR[15]	1101.2		0.12			20.25	37.00	307.0	22.40	7.96

Table 2. Elemental Analysis Results of JSO and Its Comparison with Other Samples

		element (%)						
type	sample	C	H	O	N	S	H/C	O/C
shale oil	JSO	82.24	13.68	2.62	1.31	0.16	1.99	0.024
	LK[16]	77.32	7.79	11.07	1.29	2.53	1.21	0.107
	HD[13]	85.17	12.23	1.43	0.75	0.42	1.72	0.013
	FS[14]	84.19	11.95	1.88	1.27	0.71	1.70	0.017
petroleum	TuHaC	83.66	12.60	2.21	1.24	0.29	1.81	0.020
	KVR	85.89	11.53	1.30	0.36	0.92	1.61	0.011
	TaHeR[15]	85.86	11.34	0.18	0.53	2.09	1.57	0.002

destroyed, resulting in a significant reduction in the gum content. Furthermore, Sitnov *et al.*[10] found that iron oxide nanoparticles intensify the cracking and hydrogenolysis reactions through studied effects of iron oxide nanoparticles on the aquathermolysis of oil-saturated sandstones by GC−MS and TG-DSC because the content of saturates increased and the content of resins and asphaltenes decreased significantly. Khelkhal *et al.*[11] studied the influence of Mn@Cu tallates on the oxidation process of heavy oil by GC−MS and DSC, and the results showed that Mn@Cu tallates could promote the cracking reaction of asphaltenes, resins, and other high-molecular-weight compounds to form lighter hydrocarbons. Therefore, the contents of metal ions not only affect the refining performance of oil but also have a greater impact on its utilization as chemical raw materials.

The mineral deposit of Jimusaer oil shale has been discovered and developed in recent years. Several reports on the geological exploration of the reservoir structure, formation, and sedimentation of Jimusaer oil shale have been published. However, the physical and chemical properties, chemical composition, molecular structure characteristics, and refining-processing properties of JSO are poorly understood. Therefore, this work aimed to reveal the chemical composition and molecular structure characteristics of both JSO and its group components at the microscopic level using elemental analysis (EA), thermogravimetric analysis (TG-DTG), gel chromatography (GPC), and nuclear magnetic resonance (NMR). Based on the above analysis, the semi-theoretical and semi-empirical model named structure (η)−chemical index (δ) was used to evaluate the classification of combustible minerals and processing performance in shale oil.

2. RESULTS AND DISCUSSION

2.1. Results and Discussion of JSO. *2.1.1. Basic Properties and Elemental Analysis.* Table 1 shows the basic properties and elemental analysis of JSO and other samples, which are shale oil from Longkou (LK), Huadian (HD), and Fushun (FS) and petroleum such as Tuha crude oil (TuHaC), Karamay vacuum residue (KVR), and Tahe atmospheric residue (TaHeR) in Xinjiang, China.

As shown in Table 1, for shale oil samples, the density of JSO is similar to those of HD and FS, about 900 kg/m^3. The ash content of JSO is 0.32%, which is in the middle, but still belongs to low ash oil. The moisture content of JSO is only 0.15%, which is the lowest among them, and the salt content is as high as 2.74 mg/L. Those are obviously closely related to the arid and semi-arid inland region of Xinjiang, China. The residual carbon yield of JSO is 3.27%, which is about twice higher than HD and FS, but about twice lower than LK, indicating that coking is not easy during processing JSO. The freezing point of JSO is 15 °C, which is between LK and FS, indicating that the content of paraffin in JSO is also between the two. In JSO, the content of Ni and V is much lower than those in LK, HD, and FS, and the content of Fe is also very low. The content of Ca is as high as 15.54 μg/g, which exceeds those of TuHaC and TaHeR, consistent with the previous result of salt content. Obviously, the main salt in JSO is calcium salt, and desalination pretreatment may be required before refining and processing JSO. Even so, JSO is a superior quality shale oil compared to HD, FS, and LK.

Moreover, compared with petroleum samples such as TuHaC, KVR, and TaHeR, the density of JSO is between those of TuHaC and KVR, the carbon residue rate is lower than that of TuHaC, and the total content of Ni, V, Fe, and Ca is equivalent to that of TuHaC.

Table 2 shows the results of elemental analysis of JSO and its comparison with other samples. For shale oil samples, the H/C value of JSO is 1.99, which is the highest among them. The O/C value of JSO is 0.024, which is slightly higher than those of HD and FS, but much lower than that of LK. Further, JSO has the highest N content of 1.31%. This is unfavorable since N compounds affect the oxidative stability of the oil. In contrast, the S content is only 0.16%, the lowest, which is a positive factor. Therefore, the results of elemental analysis also show that the quality of JSO is superior.

In addition, compared with the petroleum samples, the H/C value of JSO is higher than those of TuHaC, KVR, and TaHeR, the O/C value and N content of JSO are similar to those of TuHaC and much higher than those of KVR and TaHeR, and

https://doi.org/10.1021/acsomega.2c01214
ACS Omega 2022, 7, 35496−35505

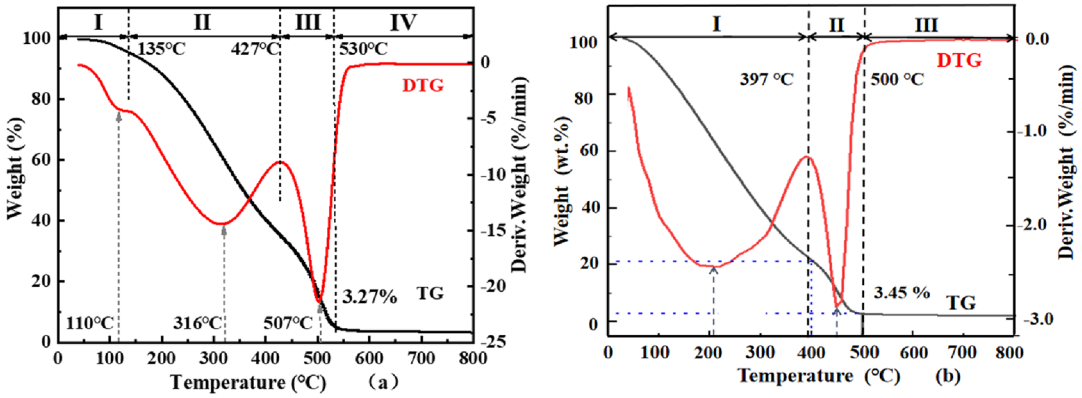

Figure 1. TG-DTG curves of JSO (a) and TuHaC (b).

the S content is the lowest. So, the quality of JSO is close to that of TuHaC and far superior to those of KVR and TaHeR.

2.1.2. TG-DTG Analysis. Figure 1 shows the TG-DTG curves of JSO (a) and TuHaC (b). As shown in Figure 1a, the mass loss process of JSO may be divided into four stages approximately, namely, temperature change ranges below 135 °C, 135−427 °C, 427−530 °C, and above 530 °C. In the first stage, the loss time is about 12.5 min, the maximum loss mass peak's temperature is about 110 °C, the loss mass rate is 4.15%/min, and the loss mass is 10.75%, which is mainly the slow escape of water and small molecules in SA. In the second stage, the loss time is about 28.4 min, the maximum loss-mass peak's temperature is about 316 °C, the loss mass rate is 14.44%/min, and the loss mass is 65.80%. Obviously, at this moment, the rest of SA and a part of AR pyrolize rapidly. In the third stage, the loss time is about 10.2 min, the maximum loss mass peak's temperature is about 508 °C, the loss mass rate is 22.54%/min, and the loss mass is 18.10%, in which the rest of AR and a small part of RE pyrolyze rapidly and the other part of RE is polycondensed.[17] In the fourth stage, the loss mass is only 2.08%, in which the rest of RE and all of AS undergo coking. The final residual carbon yield of JSO is 3.27%, which indicates that JSO has characteristics of a low condensation degree at high temperatures.[18]

As shown in Figure 1b, the mass loss process of TuHaC may be divided into three stages approximately, that is, temperature change ranges below 397 °C, 397−500 °C, and above 500 °C. In the first stage, the mass loss is as high as 78.56%, which is equivalent to the sum of the mass loss in the first and second stages of JSO. In the second stage, the mass loss is 17.99%, which is equivalent to that in the third stage of JSO. In the third stage, the mass loss is almost zero, which is equivalent to that in fourth stage of JSO. The final carbon residue yield is 3.45%, almost the same as that of JSO.

In summary, JSO and TuHaC have similar compositions and qualities because of having similar mass loss processes.

2.1.3. FT-IR Analysis. Figure 2 shows the FT-IR curve of JSO. As shown in Figure 2, its absorption peaks mainly appear in three regions, that is, 3100−2700, 1800−1200, and 900−600 cm^{-1}. Absorption peaks in the first region, which has the strongest absorption intensity among the three, belong to the characteristic absorption peak of aliphatic functional groups.[19] So, the composition of JSO is dominated by aliphatic compounds and compounds with aliphatic side chains. Absorption peaks in the second region belongs to the characteristic absorption peak of aromatic ring -C═C-. The middle-strong strong absorption intensity in this region

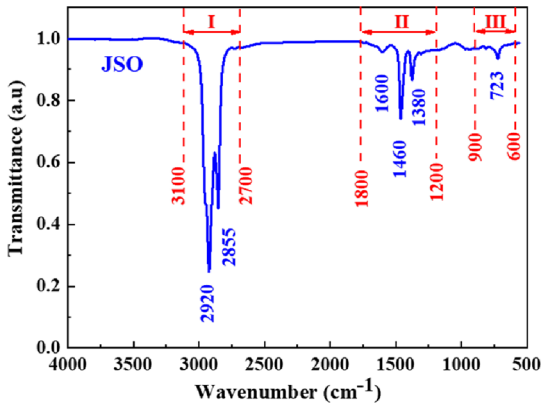

Figure 2. FT-IR spectrum of JSO.

indicates that JSO also contains a certain amount of aromatic compounds. Among them, the intensity of the characteristic peak at 1600 cm^{-1} indicates the degree of condensation of aromatic compounds,[20] and its middle-strong strong absorption intensity indicates that the content of aromatic compounds in JSO is not high and the molecular condensation degree is low. Absorption peaks in the third region are the characteristic absorption peaks of aromatic substitution. Among them, a weak absorption peak appeared at 723 cm^{-1}, indicating the presence of a small number of aromatic substituents in JSO.[21]

2.1.4. GPC Analysis. Figure 3 shows the GPC curve of JSO with its number average molecular weight (M_n) and mass average molecular weight (M_w). According to Figure 3, the M_n and M_w of JSO are 845 and 2735 g·mol^{-1}, respectively, that is,

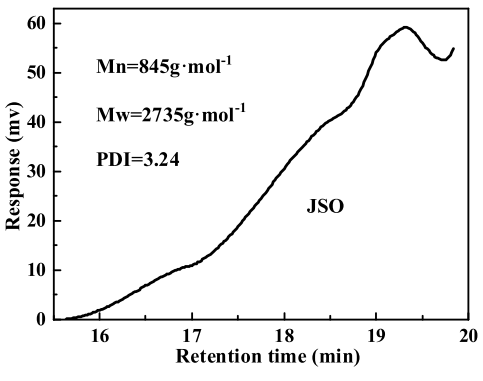

Figure 3. GPC curve of JSO.

https://doi.org/10.1021/acsomega.2c01214
ACS Omega 2022, 7, 35496−35505

the PDI value is 3.24. Combining the GPC and EA results, the average molecular formula (M_{af}) of JSO is calculated as $C_{57.91}H_{115.60}O_{1.38}N_{0.79}S_{0.04}$.

2.2. Results and Discussion of Group Components from JSO. *2.2.1. Contents of Group Components.* Figure 4 shows the contents of SA, AR, RE, and AS in JSO and its comparison with other samples. As shown in Figure 4, for shale oil samples, contents of SA, AR, RE, and AS in JSO are 54.32, 18.86, 25.81, and 1.01%, respectively, which are similar to those in FS. Obviously, SA is dominant, that is, there are more saturated hydrocarbons, which is consistent with the characteristics of a high H/C value. Also, the content of AS in JSO is only 1%, indicating that the content of thick-ring macromolecules and the association degree are both low and it is easy to process. AS will not be discussed in the follow-up study because of the very low content of AS.

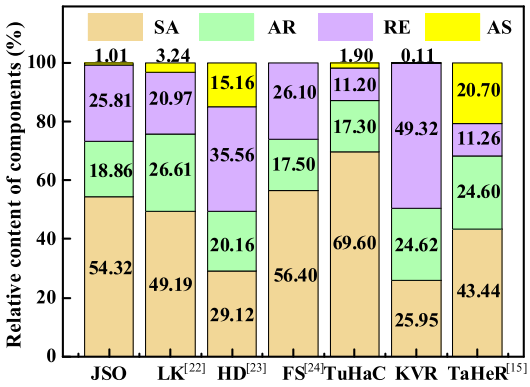

Figure 4. Contents of SA, AR, RE, and AS in JSO and its comparison with other samples.[22−24]

Further, compared with petroleum samples, for JSO, the content of SA is lower than that for TuHaC, but higher than those for KVR and TaHeR, the content of AR is comparable, and the content of RE is between those for petroleum samples, whereas the content of AS is close to those for TuHaC and KVR, which are much lower than TaHeR. This shows that the contents of group components in JSO are similar to that in TuHaC.

2.2.2. Elemental Analysis of Group Components. Table 3 shows the results of elemental analysis of SA, AR, and RE. As shown in Table 3, the H/C values of SA, AR, and RE are 2.12, 1.78, and 1.57, respectively, decreasing sequentially, indicating that the degree of molecular association increases sequentially. Also, their O/C value decreases in turn, while the N and S contents increase successively, indicating that oxygenated compounds are enriched in SA, while nitrogenous and sulfurous compounds are enriched in AR and RE. In addition, as for the distribution of metal elements, Ni, V, and Fe are mainly enriched in AR and RE, which is similar to the distribution of N and S elements. This also indicates that from SA to RE, its composition complexity increases in turn.

2.2.3. TG-DTG Analysis of Group Components. Figure 5 shows the TG (a) and DTG (b) curves of SA, AR, and RE, and Table 4 gives their pyrolysis properties. As shown in Figure 5 and Table 4, for SA, the mass loss process may be divided into three stages approximately, that is, temperature change ranges below 110 °C, 110−397 °C, and 397−500 °C. In the first stage, the loss time is about 8.02 min and the loss mass is 6.52%, which is mainly the slow escape of small molecules of alkanes from SA. In the second stage, the loss time is about 28.65 min, the maximum loss mass peak's temperature is about 303 °C, the loss mass rate is 4.43%/min, and the loss mass is 86.65%, which is mainly the pyrolysis of long-chain alkanes[25] obviously. In the third stage, the loss time is 10.30 min, the maximum loss mass peak's temperature is about 436 °C, the loss mass rate is 1.88%/min, and the loss mass is 6.59%, in which a small amount of thick-ring compounds is pyrolyzed. For AR and RE, both pyrolysis properties are similar. Their mass loss process of may be divided into three stages approximately, namely, temperature change ranges below 221 °C, 211−633 °C, and above 633 °C. In the first stage, the loss time is 19.10 min, and the loss mass values are 1.86 and 6.46%, in which alkanes and some ring aromatic compounds are pyrolyzed. In the second stage, the loss time is 41.30 min, the maximum loss mass peak's temperatures are 464 and 461 °C, the loss mass rates are 8.91 and 12.51%/min, and the loss mass values are 88.41 and 77.10%, in which intermediate-low ring aromatic compounds and thick-ring compounds are pyrolyzed. In the last stage, the loss time is 16.80 min, and the loss mass values are only 1.06 and 0.50%, in which the polycondensation of some thick-ring compounds occur. The final residual carbon yield of SA is only 0.24%, whereas those of AR and RE are 8.67 and 15.94%, respectively, indicating that during pyrolysis, SA does not condensate easily and changes into volatile products almost completely while RE condensates easily to undergo coking at high temperatures.[26]

2.2.4. FT-IR Analysis of Group Components. Figure 6 shows the FT-IR curves of SA, AR, and RE from JSO. As shown in Figure 6, the absorption peaks of SA, AR, and RE all appeared in three regions, that is, 3100−2700, 1800−1200, and 900−600 cm^{-1}, with roughly the same location but different intensities, indicating that the functional groups contained in the three are similar in structure but different in content. In the first region, the absorption peaks of SA, AR, and RE are all the strongest, indicating that there are more long-chain alkane compounds in the three. In the second region, the characteristic peaks at 1460 and 1600 cm^{-1} belong to the vibration of -C═C- in aromatic compounds, and their intensity indicates the degree of molecular condensation.[20,27] For AR and RE, the intensity of the two peaks is obviously higher than that of SA, indicating that the content of aromatic compounds and molecular condensation degree of both are higher than those of SA. In the third region, for RE, the

Table 3. Elemental Analysis of SA, AR, and RE

	element (%)										
Comp.	C	H	O	N	S	H/C	O/C	Ni (μg/g)	V (μg/g)	Fe (μg/g)	Ca (μg/g)
SA	82.09	14.50	1.58	1.70	0.13	2.12	0.014	<0.1	2.6	1.1	<0.1
AR	83.43	12.39	1.56	2.37	0.25	1.78	0.014	41.5	21.8	10.9	<0.2
RE	84.53	11.17	1.05	2.79	0.46	1.57	0.009	79.6	68.3	22.8	<0.2

https://doi.org/10.1021/acsomega.2c01214
ACS Omega 2022, 7, 35496−35505

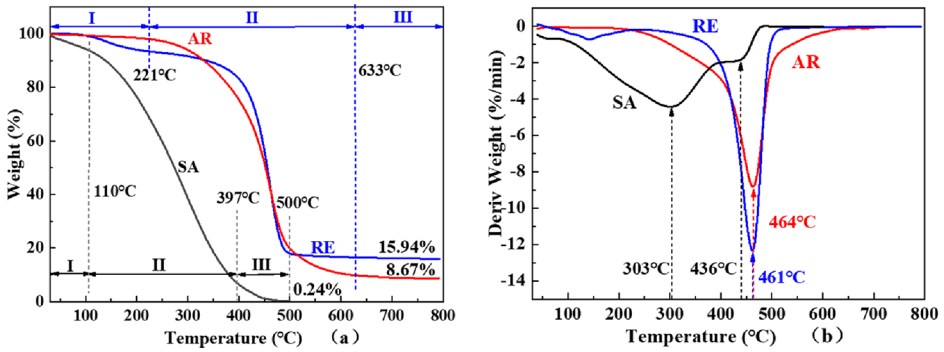

Figure 5. TG (a) and DTG (b) curves of SA, AR, and RE.

Table 4. TG-DTG Performance Analysis of SA, AR, and RE

	stage I			stage II					stage III				
Comp.	T (°C)	t (min)	loss mass (%)	T (°C)	t (min)	$T_{max\text{-}peak}$ (°C)	rate (%/min)	loss mass (%)	T (°C)	t (min)	$T_{max\text{-}peak}$ (°C)	rate (%/min)	loss mass (%)
SA	≤110	8.02	6.52	110−397	28.65	303	4.43	86.65	397−500	10.30	436	1.88	6.59
AR	≤221	19.10	1.86	221−633	41.30	464	8.91	88.41	633−800	16.80			1.06
RE			6.46			461	12.51	77.10					0.50

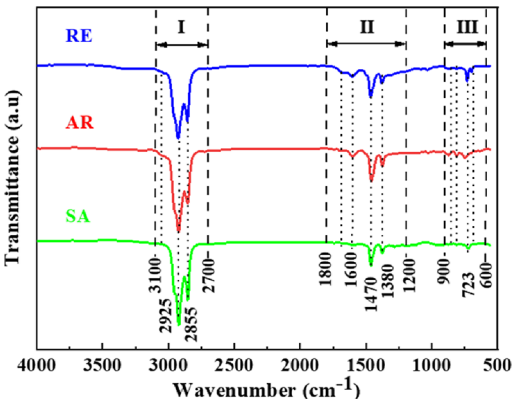

Figure 6. FT-IR spectra of SA, AR, and RE.

intensity of the peak at 723 cm^{-1} is obviously higher than those for SA and AR, indicating that the content of aromatic compounds and molecular condensation degree of both are higher than those for SA. The peak intensity of RE is significantly higher than those of SA and AR, indicating that there are more aromatic substituents in RE.

2.2.5. GPC Analysis of Group Components. Figure 7 and Table 5 give the GPC curves and M_n and M_w of SA, AR, and RE, respectively. As shown in Table 5, the M_n values of SA, AR, and RE increase successively, which are 702, 1107, and 2218 g/mol, respectively, and compared with SA, the latter two increased by 57.7 and 100%, respectively. In terms of the PDI value, SA is only 1.82, while AR and RE are 3.21 and 3.27, respectively, that is, the former is 0.78 times that of the latter two, indicating that the molecular weight distribution of SA is narrower and the difference in composition structure is smaller.

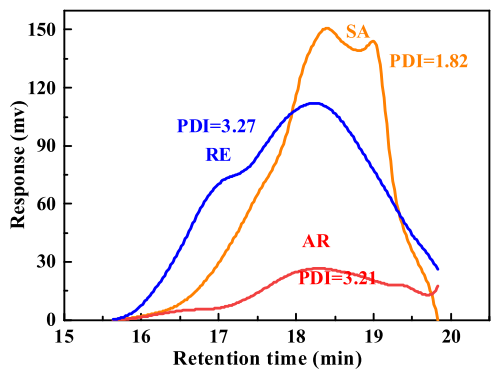

Figure 7. GPC curves of SA, AR, and RE.

Table 5. GPC Results of SA, AR, and RE

	category		
Comp.	M_n (g·mol^{-1})	M_w (g·mol^{-1})	PDI (M_w/M_n)
SA	702	1276	1.82
AR	1107	3554	3.21
RE	2218	7259	3.27

2.2.6. M_{af} of Group Components. Based on the GPC and EA results of SA, AR, and RE in Table 3 and Table 5, M_{af} of SA, AR, and RE have been calculated, and the results are given in Table 6. As shown in Table 6, in the M_{af} of SA, AR, and RE, the number of O, N, and S increases successively. Combined with the EA results in Table 3, oxygen-containing compounds are enriched in SA and AR, nitrogen-containing compounds in AR and RE, and sulfur-containing compounds in RE, whereas the S contents of SA, AR, and RE are all relatively low.

2.2.7. ^{1}H-NMR Analysis of Group Components. The ^{1}H-NMR and ^{13}C-NMR spectra of SA, AR, and RE were assigned by the "cutoff" method[28,29] because the chemical shifts cannot be accurately divided, in which their complex chemical composition and structure are similar to petroleum. Then, the relative contents of different types of hydrogen and carbon were calculated through area integration with the help of MestReNova.

Figure 8 and Table 7 show the ^{1}H-NMR spectra and their integration values of SA, AR, and RE, respectively. As shown in Table 7, in SA, AR, and RE, first of all, the H_β contents are 65.40, 56.36, and 61.02%, which are 2.23, 2.72, and 4.27 times that of H_γ, respectively, indicating that the contents of alkane or aryl alkyl substituents are decreased successively and the degree of condensation is increased sequentially. Furthermore,

https://doi.org/10.1021/acsomega.2c01214
ACS Omega 2022, 7, 35496−35505

Table 6. Elemental Analysis, M_n, and M_{af} of SA, AR, and RE

Comp.	M_n (g·mol^{-1})	element (%)					M_{af}
		C	H	O	N	S	
SA	702	82.09	14.50	1.58	1.70	0.13	$C_{48.02}H_{101.79}O_{0.69}N_{0.85}S_{0.03}$
AR	1107	83.43	12.39	1.56	2.37	0.25	$C_{76.96}H_{137.16}O_{1.08}N_{1.87}S_{0.09}$
RE	2218	84.53	11.17	1.05	2.79	0.46	$C_{156.24}H_{247.75}O_{1.46}N_{4.42}S_{0.32}$

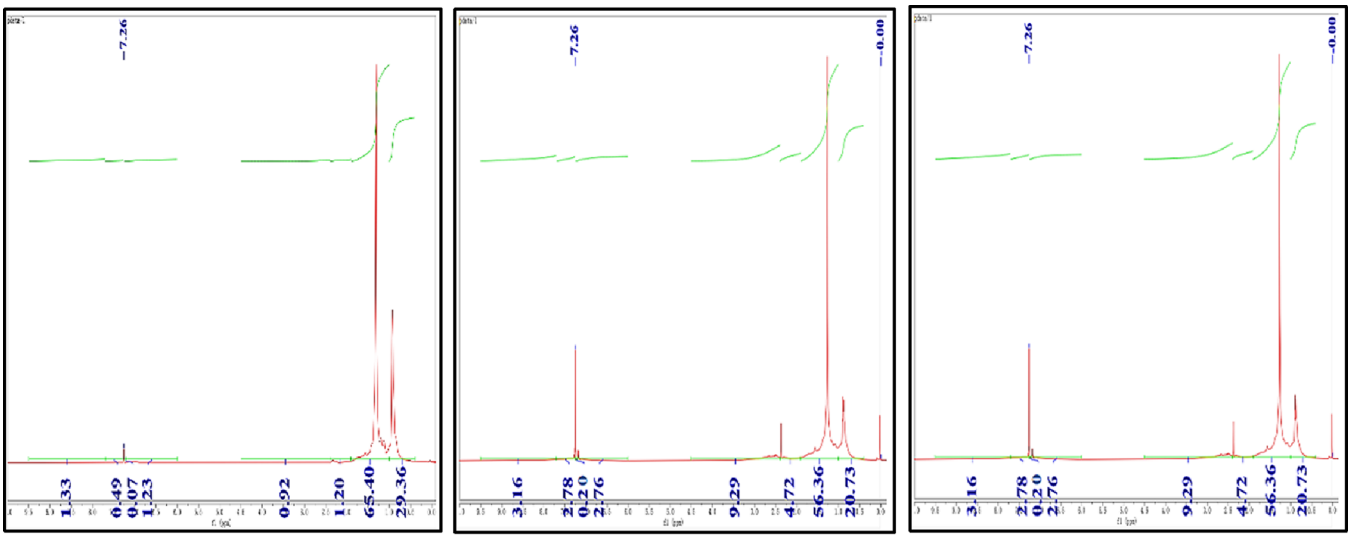

(a) (b) (c)

Figure 8. (a−c) ^{1}H-NMR spectra of SA, AR, and RE.

Table 7. Hydrogen Spectrum Attribution and Integration Results of SA, AR, and RE

symbol	description	δ_H	relative content (%)					
			SA		AR		RE	
H_γ	H in the CH_3 of aromatic γ-position and far from the γ-position, or CH_3 of alkane	0.4−1.0	29.36		20.73		14.28	
H_β	H in the CH, CH_2 aromatic β-position and far from the β-position, or in CH_3 of alkane	1.0−1.9	65.40		56.36		61.02	
H_α								
$H_{\alpha1}$	H in the α-CH_3 of aromatic	1.9−2.4	2.12	1.20	14.01	4.72	18.27	9.18
$H_{\alpha2}$	H in the α-CH_2 of aromatic	2.4−4.5		0.92		9.29		9.09
H_A								
H_{A1}	H in monocyclic aromatic	6.0−7.2	3.12	1.23	8.90	2.76	6.43	2.36
H_{A2}	H in bicyclic aromatic	7.2−7.7		0.56		2.98		1.24
	H in tricyclic and above aromatic	7.7−9.5		1.33		3.16		2.83

the H_α contents are 2.12, 14.01, and 18.27%, respectively, and the latter two are 6.61 and 8.62 times that of the former, indicating that the aromatic chain lengths of AR and RE are much higher than that of SA. Finally, the H_A contents are 3.12, 8.90, and 6.43%, respectively, and the latter two are 2.85 and 2.06 times that of the former, indicating that the degree of condensation of AR and RE is significantly greater than that of SA.

2.2.8. ^{13}C-NMR Analysis of Group Components. Figure 9 shows the ^{13}C-NMR spectra of SA, AR, and RE. In order to further explore the differences of structural characteristics of the three, the structural parameters were calculated by the modified Brown−Landner formula[30] based on Tables 7 and 8. Results are given in Table 9.

As shown in Table 8, in SA, AR, and RE, in terms of f_{ali}^C, the f_C^1 contents are 6.77, 2.41, and 1.31%, decreasing successively, and the f_C^2 contents are 10.24, 11.88, and 9.68%, roughly similar, whereas the f_C^3 contents are 80.35, 70.44, and 76.51%, respectively. This indicates that methyl carbon in the alkane chain or the chain of the aromatic cycloalkyl group decreases successively, and there are a large number of long-chain methylene groups in them, which is consistent with the results of hydrogen spectra. The f_{ar}^C contents of the three are 2.64, 15.27, and 12.50%, respectively, which are much smaller than all of f_{ali}^C in SA, AR, and RE, indicating that all of the group components are mainly composed of aliphatic chains.

Table 9 shows the calculation results of structural parameters of SA, AR, and RE. As shown in Table 9, the F_A and σ of the three are 0.01, 0.45, 0.70 and 0.25, 0.69, 0.59, respectively, increasing in sequence, which are consistent with the increasing trend of C_A, R_A, and R_N. Also, the f_P of SA is as high as 0.72, whereas the f_P values of AR and RE are only 0.18 and 0.07, indicating that SA basically does not contain aromatic and consists of chain alkanes and a few of cycloalkanes mainly, while AR and RE contain more thick-ring aromatic hydrocarbons. In addition, the σ values of AR

https://doi.org/10.1021/acsomega.2c01214
ACS Omega 2022, 7, 35496−35505

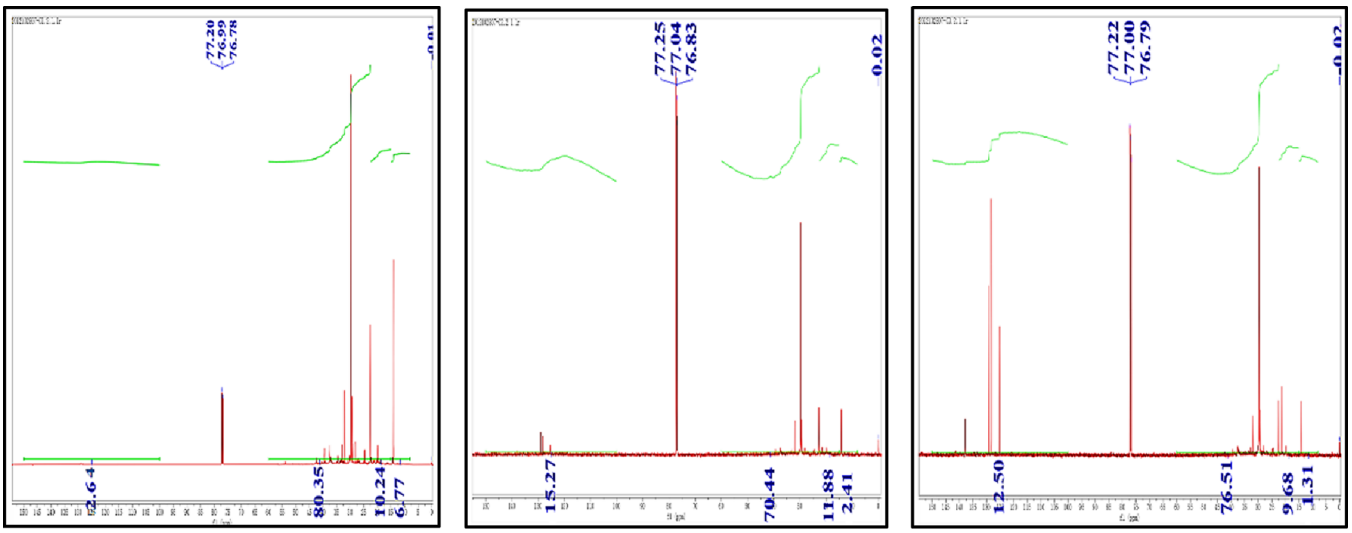

Figure 9. (a−c) ^{13}C-NMR spectra of SA, AR, and RE.

Table 8. Carbon Spectrum Attribution and Its Integration Results of SA, AR, and RE

symbol	description	δ_C	relative content (%)					
			SA		AR		RE	
f_{ali}^C								
f_C^1	C of paraffin -CH_3 or aromatic ring γ-CH_3 and γ far from -CH_3	8.0−15.0	97.36	6.77	84.73	2.41	87.50	1.31
f_C^2	C of aromatic ring α-CH_3 and β-CH_3	15.0−22.5		10.24		11.88		9.68
f_C^3	C of -CH_2 in long fatty chains or naphthenic rings	22.5−60.0		80.35		70.44		76.51
f_{ar}^C	C on aromatic ring	100.0−150.0	2.64		15.27		12.50	

Table 9. Structural Parameters Results of SA, AR, and RE

symbol	description	value		
		SA	AR	RE
f_A	aromaticity	0.01	0.45	0.70
σ	hydrogen substitution rate around aromatic rings	0.25	0.69	0.59
H_{AU}/C_A	aromatic ring condensation degree	0.0	0.68	0.64
H_T	total hydrogen number	101.79	137.16	247.75
C_S	alkyl carbon number	47.54	42.33	46.87
C_A	aromatic carbon number	0.48	34.63	109.37
R_A	aromatic ring number	0.00	8.16	26.84
R_N	naphthenic ring number	3.26	7.18	8.94
R_A/R_N	aromatic rings/naphthenic rings	0.0	1.14	3.01
C_N	naphthenic carbon number	13.04	28.72	35.76
C_P	linear alkyl carbon number	34.50	13.61	11.11
f_N	naphthenic carbon ratio	0.27	0.37	0.23
f_P	linear alkyl carbon ratio	0.72	0.18	0.07
L	average chain length	3.53	1.98	2.34
n	association degree	1.0	2.05	5.14

and RE are all higher than those of SA, which are 0.69 and 0.59, respectively, indicating that the aromatic ring side chains and association degree of group components increase successively. The H_{AU}/C_A values of the three are 0.00, 0.68, and 0.64, respectively, indicating that the aromaticity of AR and RE is much higher than that of SA. From the distribution of ring numbers, R_A and R_N increase significantly with the order of SA, AR, and RE. The N values of SA and AR are 1.0 and 2.05, respectively, while the N of RE is 5.14, which is significantly higher than the former.

2.3. Classification and Evaluation of JSO. *2.3.1. Classification of Combustible Minerals.* Based on a large number of measured data of combustible minerals such as natural gas, oil, shale oil, peat, coal, and graphite from the former Soviet Union, Dr. A.M. Zyulimayev from the Russian National Academy of Sciences proposed a semi-theoretical and semi-empirical model named structure (η)−chemical index (δ), shown in Figure 10, to judge the universality of combustible minerals.[31] As shown in Figure 10, the values of δ and η vary from −12.5 to 16.67 and 0 to 5, respectively, and η has a linear relationship with δ. There are four regions, namely, the gas

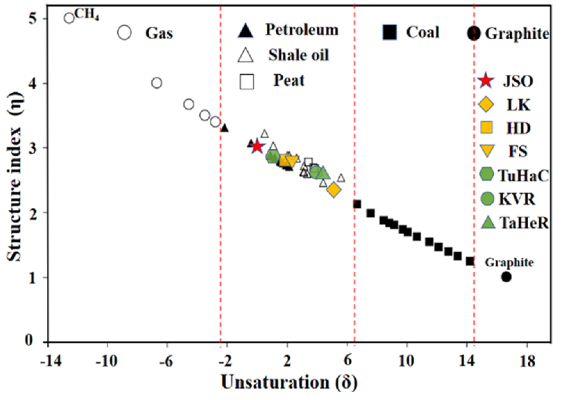

Figure 10. Locations of JSO and other samples in the empirical classification plot of combustible minerals based on δ−η.

https://doi.org/10.1021/acsomega.2c01214
ACS Omega 2022, 7, 35496−35505

region, oil−peat region, coal region, and graphite region. Furthermore, with the increase in δ, the order of combustible minerals is natural gas (starting point), petroleum, shale oil, peat, coal, and graphite (end point).

The model is based on the elemental analysis (EA) results of combustible minerals. Taking a 1 g sample as the calculation basis, δ and η are calculated through eqs 1−4.

$$N_{aT} = N_C + N_H + N_O + N_N + N_S \quad (1)$$

$$N_{CB} = 2N_C + \frac{(N_H + 3N_N)}{2} + N_O + N_S \quad (2)$$

$$\delta = 2(N_{CB} - N_{aT}) \quad (3)$$

$$\eta = \frac{N_{aT}}{N_C} \quad (4)$$

where N_i (i = C, H, O, N, and S) refers to the atom number of the i element in the sample (wt %), N_{aT} refers to the total atom number, N_{CB} refers to the total number of chemical bonds, δ refers to the unsaturation, and η refers to the structure index.

According to the values in Table 2, N_C, N_H, N_O, N_N, and N_S of JSO and other oil samples were calculated respectively, and then, N_{aT}, N_{CB}, δ, and η were calculated through eqs 2−5, respectively. The results are listed in Table 10 and plotted in Figure 10.

Table 10. δ and η Results of JSO and Other Samples

		symbol			
type	sample	N_{aT}	N_{CB}	δ	η
shale oil	JSO	20.80	20.86	0.12	3.03
	LK	15.10	17.69	5.19	2.34
	HD	19.48	20.49	2.02	2.75
	FS	19.20	20.28	2.17	2.74
petroleum	TuHaC	19.81	20.52	1.43	2.84
	KVR	18.82	20.23	2.81	2.63
	TaHeR	18.61	20.11	3.01	2.60

As shown in Figure 10, JSO falls into the upper part of the oil−peat region and is close to TuHaC, indicating that JSO has similar composition to petroleum and belongs to a better shale oil. HD and FS fall into the lower part of the oil−peat region, indicating that they are typical shale oil with a better quality than KVR and TaHeR. Meanwhile, LK is close to the peat location, indicating that its quality is lower than those of KVR and TaHeR.

2.3.2. Evaluation of Processing Performance. Figure 11 shows the empirical classification diagram of petroleum refining-processing performance.[32] As shown in Figure 11, according to the basic properties of the samples in Table 1, the sum of V and Ni contents is 21.57 μg/g, and the carbon residue yield is 3.27% in JSO, which is in the easy processing area, that is, JSO has excellent refining-processing performance, whereas LK, HD, and FS fall into the slightly difficult processing region, indicating that their refining-processing performance is inferior to JSO. Moreover, KVR and TaHeR fall into the not difficult and the difficult processing region, respectively. In conclusion, the refining-processing performance JSO and TuHaC are the best followed by KVR, LK, HD, and FS, and TaHeR is the worst one.

The contents of Ni, V, Fe, and Ca in JSO not only affect the refining performance of JSO oil but also have a greater impact

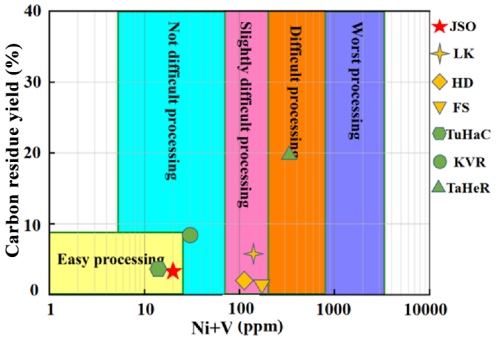

Figure 11. Processing performance of JSO and other samples.

on its utilization as chemical raw materials. Therefore, further studies are planned on the occurrence forms of various metal elements in JSO and its group components, especially the existing forms of the Ca element in JSO, so as to provide scientific basis for the removal and utilization of these metal elements.

3. CONCLUSIONS

This paper demonstrated the first chemical structure and composition and refining performance of shale oil collected from Jimusaer, Xinjiang, China. We focused on the character of JSO as a raw material for the preparation of fine chemicals in addition to an energy resource. Several meaningful conclusions were made as listed in the following:

(1) In terms of basic properties, metal content, H/C, O/C, N, and S content, combustible mineral classification and refining-processing performance, JSO is a high-quality shale oil with excellent refining-processing performance compared with shale oil sampled from other areas such as LK, HD, and FS.

(2) JSO is also a superior oil sample compared with petroleum since it has eidentical thermogravimetric processes, total metal contents, and refining properties compared with TuHaC.

(3) For the contents of group components, JSO with SA as a dominant component is closer to FS in the shale oil group samples. In the petroleum oil group, JSO is closer to TuHaC.

(4) The results of ^{1}H-NMR analysis demonstrated that the substitution sites of alkanes or aryl groups of SA, AR, and RE decrease in turn. However, the degree of condensation of these three group components increases. The length of aromatic side chains and the degree of condensation of aromatic rings of the AR and RE are much higher than SA. Additionally, the ^{13}C-NMR analysis indicated that SA mainly consists of chain alkanes with a few cycloalkanes, whereas AR and RE contain more content of thick-ring aromatic hydrocarbons. R_A and R_N increase significantly, which indicated that the association degree of RE is significantly higher than those of SA and RE.

(5) According to the GPC analysis, the M_n values of JSO, SA, AR, and RE are 845, 702, 1107, and 2218 g·mol^{-1}, respectively. Based on the results of GPC and EA, their M_{af} are $C_{57.91}H_{115.60}O_{1.38}N_{0.79}S_{0.04}$, $C_{48.02}H_{101.79}O_{0.69}N_{0.85}S_{0.03}$, $C_{76.96}H_{137.16}O_{1.08}N_{1.87}$ $S_{0.09}$, and $C_{156.24}H_{247.75}O_{1.46}$ $N_{4.42}S_{0.32}$, respectively.

https://doi.org/10.1021/acsomega.2c01214
ACS Omega 2022, 7, 35496−35505

This study revealed the chemical composition and molecular characteristics of JSO from the microscopic level. It can act as the cornerstone of understanding and utilization of JSO in the future.

4. MATERIALS AND METHODS

4.1. Materials. The oil shale with an oil content about 10% was taken from Jimusaer, Xinjiang, China. JSO is obtained from the oil shale by dry distillation at about 500 °C.

Chemicals used in the experiment were toluene, *n*-heptane, absolute ethanol, (all analytically pure, Tianjin Yongsheng Fine Chemical Co., Ltd.) and neutral alumina (analytically pure, Tianjin Zhiyuan Chemical Reagent Co., Ltd.). Before filling the chromatographic column, the neutral alumina was activated at 500 °C for 6 h.

4.2. Experimental Methods. Figure 12 shows the process of separating group components of SA, AR, RE, and AS from

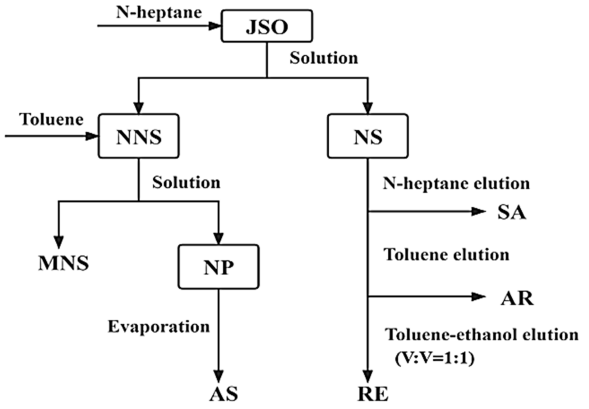

Figure 12. Process of separation group components from JSO.

JSO. As shown in Figure 12, under the conditions of a solution/oil ratio of 25:1 (m/m) and time of 48 h, *n*-heptane-soluble (NS) and *n*-heptane-insoluble (NNS) samples were separated by Soxhlet dissolution. Then, NS was separated through column chromatography, and SA by *n*-heptane, AR by toluene, and RE by a mixture solvent of toluene and ethanol (v/v = 1:1) were obtained successively, whereas the toluene-soluble (NP) sample, namely, asphaltene (AS), was separated from NNS by toluene, and the residuum was toluene insoluble (MNS).

Then, SA, AR, RE, and AS were placed in the rotary evaporator to recover the solvent, dried at 110 °C under vacuum for 2 h, and weighed (m_i). According to eq 5, the yield (Y_i) of SA, AR, RE, and AS was calculated.

$$Y_i = \frac{m_i}{m_o} \times 100\% \quad (5)$$

where m_i (g) refers to the mass of SA, AR, RE, or AS and m_o (g) refers to the mass of JSO.

4.3. Analytical Methods. C, H, O, N, and S contents were determined by a Vario EL III elemental analyzer (Elementar, Germany), and Ni, V, Fe, and Ca contents were tested by a Z8000 plasma emission spectrometer (PE, USA). TG-DTG analysis was performed by an SDT-Q600 thermogravimetric analyzer (TA, USA) under the conditions of a N_2 atmosphere, sample mass of 5 mg, heating rate of 10 °C/min, and final temperature of 800 °C. FT-IR was tested by a VERTEX-70 (Bruker Germany). Spectra were obtained between 500 and 4000 cm^{-1}, and a resolution of 0.01 cm^{-1} was used. The relative molecular weight was determined by an Agilent-11006 (Agilent, USA) under the conditions of a sample mass of 2 mg, tetrahydrofuran being a solvent, a flow rate of 0.6 mL/min, and a column temperature of 40 °C. Using a Varian Inova-400 superconducting NMR instrument (Varian, USA), deuterated chloroform as a solvent, and tetramethylsilane an internal standard, ^{1}H-NMR and ^{13}C-NMR of samples were analyzed at ambient temperature.

AUTHOR INFORMATION

Corresponding Authors

Aisha Nulahong − *State Key Laboratory of Chemistry and Utilization of Carbon-Based Energy Resources, School of Chemical Engineering and Technology and College of Chemical Engineering, Xinjiang University, Urumqi, Xinjiang 830017, China*; Phone: 13639930652; Email: aisa705@163.com

Fengyun Ma − *State Key Laboratory of Chemistry and Utilization of Carbon-Based Energy Resources, School of Chemical Engineering and Technology, Xinjiang University, Urumqi, Xinjiang 830017, China*; Phone: 13999135771; Email: ma_fy@126.com

Authors

Luhao Chen − *State Key Laboratory of Chemistry and Utilization of Carbon-Based Energy Resources, School of Chemical Engineering and Technology and College of Chemical Engineering, Xinjiang University, Urumqi, Xinjiang 830017, China*

Jingmei Liu − *State Key Laboratory of Chemistry and Utilization of Carbon-Based Energy Resources, School of Chemical Engineering and Technology and College of Chemistry, Xinjiang University, Urumqi, Xinjiang 830017, China*

Zhilei Wu − *State Key Laboratory of Chemistry and Utilization of Carbon-Based Energy Resources, School of Chemical Engineering and Technology and College of Chemical Engineering, Xinjiang University, Urumqi, Xinjiang 830017, China*

Jinsheng Liu − *Xinjiang Modern Petrochemical Co., Ltd., Urumqi, Xinjiang 831499, China*

Complete contact information is available at: https://pubs.acs.org/10.1021/acsomega.2c01214

Notes

The authors declare no competing financial interest.

REFERENCES

(1) Han, X.; Indrek, K.; Jiang, X. M.; Suuberg, E. M. Review of oil shale semicoke and its combustion utilization. *J. Fuel.* **2014**, *126*, 143−161.

(2) Wang, Q.; Liu, Q.; Wang, Z. C.; Liu, H. P.; Bai, J. R.; Ye, J. B. Characterization of organic nitrogen and sulfur in the oil shale kerogens. *Fuel Process. Technol.* **2017**, *160*, 170−177.

(3) Daniel, J. S. The successful development of gas and oil resources from shales in North America. *J. Pet. Sci. Eng.* **2018**, *163*, 399−420.

(4) Zhang, X.; Liu, J. Y.; Hou, P. F. A review on the for mation and distribution theories of the shale oil in China. *J. Geol. Resources.* **2019**, *28*, 165−170.

(5) Jacqueline, M. J.; Justin, M.; Billing, R. T.; Andrew, J. S.; Tanner, M. S. Hydrothermal Liquefaction Biocrude Compositions Compared to Petroleum Crude and Shale Oil. *J. Energy Fuels.* **2017**, *31*, 2896−2906.

https://doi.org/10.1021/acsomega.2c01214
ACS Omega 2022, 7, 35496−35505

(6) Kholoud, M.; Yahya, A.-D.; Saif, A.-Z.; Abdullah, S. Extraction and fractionation of organic matters from Jordanian-origin oil shale under different operational parameters. *J. Pet Sci Technol.* **2022**, *20*, 1−21.
(7) Li, Xu. *Study on separation and analysis of shale oil components extracted by near critical water*; D. Jilin University, 2014.
(8) Cui, D.; Wang, Q.; Wang, Z. C.; Liu, Q.; Pan, S.; Bai, J.; Liu, B. Compositional Analysis of Heteroatom Compounds in Huadian Shale Oil Using Various Analytical Techniques. *J. Energy Fuels.* **2019**, *33*, 946−956.
(9) Irek, I. M.; Indad, S. S.; Mohammed, A. K.; Alexey, V. V. Application of Aromatic and Industrial Solvents for Enhancing Heavy Oil Recovery from the Ashalcha Field. *J. Energy Fuels.* **2021**, *35*, 374−385.
(10) Sergey, S.; Irek, M.; Firdavs, A.; Mohammed, A. K.; Olga, S.; Konstantin, B. Heavy oil aquathermolysis in the presence of rock-forming minerals and iron oxide (II, III) nanoparticles. *J. Pet. Sci. Technol.* **2020**, *38*, 574−579.
(11) Mohammed, A. K.; Alexey, A. E.; Danis, K. N.; Alexey, V. V. Thermal Study on Stabilizing the Combustion Front via Bimetallic Mn@Cu Tallates during Heavy Oil Oxidation. *J. Energy Fuels.* **2020**, *34*, 5121−5127.
(12) He, L.; Ma, Y.; Tan, T.; Yue, C.; Li, S.; Tang, X. Mechanisms of sulfur and nitrogen transformation during Longkou oil shale pyrolysis. *J. Energy.* **2021**, *232*, 1−13.
(13) Chang, Z.; Chu, M. The chemical composition and pyrolysis characteristics of thermal bitumen derived from pyrolyzing Huadian oil shale. *China. J. Oil Shale.* **2019**, *36*, 62−75.
(14) Ding, H.; Ma, Y.; Li, S.; Wang, Q.; Hong, W.; Jiang, M. Structural characterization of thermal bitumen extracted from Fushun oil shale semi-coke with ionic liquid N-methyl pyrrolidone. *J. Therm. Anal. Calorim.* **2021**, *146*, 1613−1622.
(15) Hong, K.; Ma, F. Y.; Liu, J. M.; Zhong, M. Study on noisothermal thermal conversion reaction performance of Tahe atmospheric residue and its group components. *J. Pet. Refin. Chem. Ind.* **2015**, *46*, 34−38.
(16) Zhang, Z.; Guo, L.; Zhan, J.; Zhan, J. H. Comparing product distribution and desulfurization during direct pyrolysis and hydro-pyrolysis of Longkou oil shale kerogen using reactive MD simulations. *J. Hydrogen Energy* **2019**, *44*, 25335−25346.
(17) Hong, K.; Ma, F. Y.; Zhong, M.; Liu, J. M. Study on hydro thermal conversion reaction performance of Tahe atmospheric residue and its remove-asphaltene oil. *J. Pet. Refin. Chem. Ind.* **2016**, *47*, 34−38.
(18) Jeffrey, L. B.; John, Q.; Marco, J. C. Investigating Secondary Pyrolysis Reactions of Coal Tar via Mass Spectrometry Techniques. *J. Energy Fuels.* **2017**, *31*, 1269−1275.
(19) Bin, C.; Han, X.; Jiang, X. In Situ FT-IR Analysis of the Evolution of Functional Groups of Oil Shale During Pyrolysis. *J. Energy Fuels.* **2016**, *30*, 5611−5616.
(20) Wang, Q.; Cui, D.; Wang, P.; Bai, J.; Wang, Z.; Liu, B. A comparison of the structures of >300 °C fractions in six Chinese shale oils obtained from different locations using ^{1}H-NMR, ^{13}C-NMR and FT-IR analyses. *J. Fuel.* **2018**, *211*, 341−352.
(21) Shan, X.-K.; Zhao, S.-L.; Ma, Y.-Y.; Mo, W.; Wei, X.-Y. Analysis of Pyrolysis Performance and Molecular Structure of Five Kinds of Low-Rank Coals in Xinjiang Based on the TG-DTG Method. *J. ACS Omega.* **2022**, *7*, 8547−8557.
(22) Wang, W.; Ma, Y.; Li, S.; Yue, C.; Wu, J.; Teng, J. Pyrolysis characteristics of Longkou oil shale under optimized condition. *J. Therm. Anal. Calorim.* **2016**, *125*, 983−990.
(23) Guo, W.; Yang, Q. C.; Sun, Y. H.; Xu, S. T.; Kang, S. J.; Lai, C.; Guo, M. Y. Characteristics of low temperature co-current oxidizing pyrolysis of Huadian oil shale. *J. Anal. Appl. Pyrol.* **2020**, *146*, 1−7.
(24) Zhao, X.; Liu, Z.; Lu, Z.; Shi, L.; Liu, Q. A study on average molecular structure of eight oil shale organic matters and radical information during pyrolysis. *J. Fuel.* **2018**, *219*, 399−405.
(25) Mohammed, A. K.; Semen, E. L.; Nikita, E. I.; Alexey, A. E.; Mikhail, Y. G.; Nikolay, Y. P.; Tatiana, O. K.; Alexey, V. V. A Thermal Study on Peat Oxidation Behavior in the Presence of an Iron-Based Catalyst. *J. Catalysts.* **2021**, *11*, 1344−1360.
(26) Xu, Y.; Zhang, G. J.; Zhang, X. D.; Zhang, Y. F. The characteristics and mechanism for the formation of tars from low temperature pyrolysis of lignite. *J. Energy Inst.* **2021**, *99*, 248−255.
(27) Sun, Z. Q.; Ma, F. Y.; Liao, J.; Liu, J. M.; Zhong, M.; Kong, L. T. Effects of mechanical activation on the co-liquefaction of Xigou sub-bituminous coal from Xinjiang and Karamay petroleum vacuum residues. *J. Fuel Process. Technol.* **2017**, *161*, 139−144.
(28) Calemma, V.; Rausa, P.; D'Antona, L.; Montanari, L. Characterization of Asphaltenes Molecular Structure. *J. Energy Fuels* **1998**, *12*, 422−428.
(29) Abdul Jameel, A. G.; Elbaz, A. M.; Emwas, A. H.; Roberts, W. L.; Sarathy, S. M. Calculation of Average Molecular Parameters, Functional Groups, and a Surrogate Molecule for Heavy Fuel Oils Using ^{1}H and ^{13}C Nuclear Magnetic Resonance Spectroscopy. *J. Energy Fuels* **2016**, *30*, 3894−3905.
(30) Wang, Z. C.; Ge, Y.; Shui, H. F.; Ren, S. B.; Pan, C. X.; Kang, S. G.; Lei, Z. P.; Zhao, Z. J.; Hu, J. C. Molecular structure and size of asphaltene and preasphaltene from direct coal liquefaction. *J. Fuel Process. Technol.* **2015**, *137*, 305−311.
(31) Julimariev, A. M.; Golovin, G. Classification and application of coal structure chemical index. *M.* **2013**.
(32) Yu, C. Z. Industrial application and optimization of residue hydrodesulfurization catalyst grading scheme. *D. China Univ. Pet.* **2009**.

https://doi.org/10.1021/acsomega.2c01214
ACS Omega 2022, 7, 35496−35505